HFF
8,5

504

Received September 1996
Revised November 1997
Accepted January 1998

# Free convection in micropolar fluids over a uniformly heated vertical plate

Rama Subba Reddy Gorla
*Department of Mechanical Engineering, Cleveland State University, Cleveland, Ohio, USA*
A. Slaouti
*Department of Mechanical Engineering, Manchester Metropolitan University, Manchester, UK, and*
H.S. Takhar
*School of Engineering, University of Manchester, Manchester, UK*

## Nomenclature

| | | |
|---|---|---|
| $f$ | = | dimensionless velocity function |
| $g$ | = | dimensionless microrotation |
| $g$ | = | acceleration due to gravity |
| $G^*$ | = | modified Grashof number parameter |
| $Gr_x^*$ | = | Grashof number |
| $h$ | = | heat transfer coefficient |
| $j$ | = | microinertia per unit mass |
| $k$ | = | thermal conductivity of the fluid |
| $M_w$ | = | local couple stress |
| $n$ | = | constant |
| $N$ | = | angular velocity |
| $Nu$ | = | Nusselt number |
| $Pr$ | = | Prandtl number |
| $q_w$ | = | surface heat flux |
| $T$ | = | temperature |
| $u,v$ | = | velocity components |
| $x,y$ | = | distance along and normal to the surface |
| $\psi$ | = | stream function |
| $\mu$ | = | viscosity coefficient |
| $\rho$ | = | density of the fluid |
| $\kappa$ | = | rotational viscosity coefficient |
| $\beta$ | = | volumetric coefficient of expansion |
| $\gamma$ | = | gyroviscosity coefficient |
| $\xi,\eta,\chi$ | = | dimensionless coordinates |
| $\theta$ | = | dimensionless temperature |
| $\Delta$ | = | dimensionless material property |

*Subscripts*

| | | |
|---|---|---|
| $w$ | = | surface conditions |
| $\infty$ | = | reference conditions |

## Introduction

Free convection flow is caused by buoyancy forces which arise from density differences in a fluid. These density differences are a consequence of temperature gradients within the fluid. Free convection flow is a significant factor in several practical applications which include, for example, cooling of electronic components.

There exist relatively few studies concerning the non-Newtonian fluids with microstructures such as polymeric additives, colloidal suspensions, animal blood, liquid crystals etc. Eringen (1966) developed the theory of micropolar fluids which show microrotation effects as well as microinertia. The theory of thermomicropolar fluids was developed by Eringen (1972) by extending the

International Journal of Numerical Methods for Heat & Fluid Flow
Vol. 8 No. 5, 1998, pp. 504–518.
© MCB University Press, 0961-5539

The authors are grateful to the reviewers for their helpful comments.

theory of micropolar fluids. Gorla (1983) investigated the forced convective heat transfer to a micropolar fluid flow over a flat plate. The free convective heat transfer to a thermomicropolar fluid along a vertical flat plate was studied by Jena and Mathur (1981) by means of similarity arguments.

In this paper, we have studied the nonsimilar problem of natural convection boundary layer flow of a micropolar fluid over a vertical plate with uniform heat flux boundary condition. The numerical results revealed the presence of a two-layer structure as the distance from the leading edge increases. The existence of an inner layer close to the wall is due to the restriction imposed by the wall on the rotation of the microelements in the fluid, as explained by Rees and Bassom (1996). An asymptotic analysis for large distances away from the leading edge is presented since accurate numerical results are difficult to obtain in this region because of the near-wall regime. Numerical results for the friction factor and Nusselt number are presented for different values of the material parameters and Prandtl number of the fluid.

**Governing equations**

Consideration is given to a vertical heated plate immersed in a micropolar fluid with a uniform temperature $T_\infty$. The governing equations for the steady, laminar, incompressible, micropolar fluid may be written within the boundary layer and Boussinesq approximations as:

$$\frac{\partial u}{\partial x}+\frac{\partial v}{\partial y}=0 \tag{1}$$

$$\rho\left(u\frac{\partial u}{\partial x}+v\frac{\partial u}{\partial y}\right)=(\mu+\kappa)\frac{\partial^2 u}{\partial y^2}+\kappa\frac{\partial N}{\partial y}+\rho g\beta(T-T_\infty) \tag{2}$$

$$\rho j\left(u\frac{\partial N}{\partial x}+v\frac{\partial N}{\partial y}\right)=-\kappa\left(2N+\frac{\partial u}{\partial y}\right)+\gamma\frac{\partial^2 N}{\partial y^2} \tag{3}$$

$$u\frac{\partial T}{\partial x}+v\frac{\partial T}{\partial y}=\alpha\frac{\partial^2 T}{\partial y^2} \tag{4}$$

The boundary conditions may be written as

$$y=0: \quad u=v=0,\ N=-n\frac{\partial u}{\partial y},\ \frac{\partial T}{\partial y}=-\frac{q_w}{k} \tag{5}$$

$$y\to\infty: \quad u\to 0, N\to 0, T\to T_\infty$$

In the above equations, $x$ and $y$ are the coordinates measured along and perpendicular to the plate; $u$ and $v$ the velocity components in x and y directions; $N$ the microrotation component in the $x$-$y$ plane; $\rho$ the density; $\mu$ the

coefficient of viscosity; $\kappa$ the rotational viscosity coefficient; $\gamma$ the gyroviscosity coefficient; $j$ the microinertia density; $\alpha$ the thermal diffusivity and $T$ the temperature of the fluid.

A comment will be made on the boundary condition used for the microrotation term. When $n = 0$, equation (5) yields $N(x,0) = 0$. This represents the case of concentrated particle flows in which the microelements close to the wall are not able to rotate. The case corresponding to $n = 1/2$ results in the vanishing of antisymmetric part of stress tensor and represents weak concentrations. The particle spin is equal to fluid vorticity at the boundary for the fine particle suspensions. The case corresponding to $n = 1$ is representative of turbulent boundary layer flows. Thus for $n = 0$, particles are not free to rotate near the surface, whereas, as $n$ increases from 0 to 1, the microrotation term gets augmented and induces flow enhancement

We define a stream function $\Psi(x,y)$ such that

$$u = \frac{\partial \Psi}{\partial y} \quad and \quad v = -\frac{\partial \Psi}{\partial x}.$$

The continuity equation (1) is then automatically satisfied. Proceeding with the analysis, we define the following dimensionless transformations:

$$\eta = \frac{y}{5x} G^*$$

$$\xi = \frac{25x^2}{(G^*)^2}$$

$$G^* = 5(G^*_{rx}/5)^{1/5}$$

$$G^*_{rx} = \frac{g\beta q_w x^4}{k\nu^2}$$

$$\Psi = \nu G^* f(\xi, \eta)$$

$$N = \frac{\nu (G^*)^3}{25x^2} g(\xi, \eta)$$

$$\theta = \frac{T - T_\infty}{[\frac{5xq_w}{kG^*}]} \tag{6}$$

On substituting the expressions in equation (6) into equations (2)-(5), we have

$$(1+\Delta)f''' + 4ff'' - 3(f')^2 + \Delta g' + \theta = 2\xi\left[f'\frac{\partial f'}{\partial \xi} - f''\frac{\partial f}{\partial \xi}\right] \tag{7}$$

$$\left(1+\frac{\Delta}{2}\right)g'' + 4fg' - 2f'g - \Delta\xi\,(2g + f'') = 2\xi\left[f'\frac{\partial g}{\partial \xi} - g'\frac{\partial f}{\partial \xi}\right] \tag{8}$$

$$\frac{\theta''}{\mathrm{Pr}} + 4f\theta' - f'\theta = 2\xi\left[f'\frac{\partial \theta}{\partial \xi} - \theta'\frac{\partial f}{\partial \xi}\right]) \tag{9}$$

The transformed boundary conditions are given by

$$\eta = 0: \quad f = f' = 0,\ g = -nf'',\ \theta' = -1$$
$$\eta \to \infty: \quad f' = 0,\ g = 0,\ \theta = 0 \tag{10}$$

In the above equations, a prime indicates differentiation with respect to $\eta$ only.

The wall shear stress may be written as

$$\tau_w = [(\mu + \kappa)\frac{\partial u}{\partial y} + \kappa N]_{y=0} \tag{11}$$

The local friction factor is defined as

$$C_{fx} = \frac{2}{G^*}[1 + (1-n)\Delta]f''(\xi, 0) \tag{12}$$

The local couple stress at the wall is given by

$$M_w = \gamma\left(\frac{\partial N}{\partial y}\right)_{y=0} = \frac{\gamma (G^*)^4}{125x^3}g'(\xi, 0) \tag{13}$$

The local heat transfer coefficient is given by

$$h_x = \frac{q_w(x)}{T_w - T_\infty} = \frac{kG^*}{5x\theta(\xi, 0)} \tag{14}$$

The local Nusselt number is given by

$$N_{ux} = \frac{hx}{k} = \frac{G^*}{5\theta(\xi, 0)} \tag{15}$$

The case corresponding to $\Delta = 0$ gives a similarity solution. This is governed by the following set of equations:

$$f''' + 4ff'' - 3(f')^2 + \theta = 0 \tag{16}$$

$$g''+4f\,g'-2f'g=0 \tag{17}$$

$$\frac{\theta''}{\mathrm{Pr}}+4f\theta'-f'\theta=0 \tag{18}$$

**Numerical scheme**

The numerical scheme to solve equations (7)-(9) is based on the following concepts:

(a) The boundary conditions for $\eta = \infty$ are replaced by

$$f'(\xi,\eta_{\max})=0,\ g(\xi,\eta_{\max})=0,\ \theta(\xi,\eta_{\max})=0 \tag{19}$$

where $\eta_{\max}$ is a sufficiently large value of $\eta$ where the boundary condition for velocity field is satisfied. After confirming that setting $\eta_{\max}$ to higher values would not change the results obtained, we have set $\eta_{\max} = 25$.

(b) The two-dimensional domain of interest, $(\xi,\eta)$ is discretized with an equispaced mesh in the $\xi$ direction and another equispaced mesh in the $\eta$ direction.

(c) The partial derivatives with respect to $\xi$ and $\eta$ are all valued by the central difference approximations.

(d) Two iteration loops based on the successive substitution are used because of the nonlinearity of the equations.

(e) In each inner iteration loop, the value of $\xi$ is fixed while each of equations (7)-(9) is solved as a linear second-order boundary value problem of ODE on the $\eta$ domain. The inner iteration is continued until the nonlinear solution converges for the fixed value of $\xi$.

(f) In the outer iteration loop, the value of $\xi$ is advanced from 0 to 5. The derivatives with respect to $\xi$ are updated after every outer iteration step.

More details on the numerical scheme are explained in Gorla *et al.* (1993). The numerical results are affected by the number of mesh points in both directions. To obtain accurate results, a mesh sensitivity study was performed. In the $\eta$ direction, after the results for the mesh points 51, 100, 200 and 800 were compared, it was found that 200 points gave the same results as 800. On the $\xi$ direction 51 mesh points were found to give accurate results. Therefore, the computations were performed with ( $200 \times 51$) mesh points.

**Asymptotic solution**

Here, we investigate the boundary layer behavior at large distances away the leading edge.

We now define

$$h = g + \frac{f''}{2} \tag{20}$$

$$\chi = \eta \xi^{1/2}$$

Substituting expressions in equation (20) into equations (7)-(9) we have

$$(1+\frac{\Delta}{2}) f''' + 4\xi^{-\frac{1}{2}} f f'' - 3\xi^{-\frac{1}{2}} (f')^2 + \Delta \xi^{-1} h' + \xi^{-\frac{3}{2}} \theta = 2\xi^{\frac{1}{2}} [f' \frac{\partial f'}{\partial \xi} + f'' \frac{\partial f}{\partial \xi}] \tag{21}$$

$$(1+\Delta) h'' + \frac{\xi^{-\frac{1}{2}} \theta'}{2} + 4\xi^{-\frac{1}{2}} f h' - 2\xi^{-\frac{1}{2}} f' h - 2\Delta h = 2\xi^{\frac{1}{2}} [f' \frac{\partial h}{\partial \xi} - h' \frac{\partial f}{\partial \xi}] \tag{22}$$

$$\frac{\theta''}{\mathrm{Pr}} + 4\xi^{-\frac{1}{2}} f \theta' - \xi^{-\frac{1}{2}} f' \theta = \xi^{\frac{1}{2}} [f' \frac{\partial \theta}{\partial \xi} - \theta' \frac{\partial f}{\partial \xi}] \tag{23}$$

on equations (21)- (23), a prime denotes differentiation with respect to $\chi$. The boundary conditions at $\chi = 0$ are given by

$$\chi = 0: \qquad f = f' = 0, \quad h = (\frac{1}{2} - n) f'' \xi, \quad \theta' = -\xi^{-\frac{1}{2}} \tag{24}$$

we now set for the main layer equations (7)-(9) the following expansion:

$$f(\xi, \eta) = F_0(\eta) + \xi^{-\frac{1}{2}} F_1(\eta) + \ldots$$

$$h(\xi, \eta) = \xi^{-1} H_0(\eta) + \xi^{-3/2} H_1(\eta) + \ldots \tag{25}$$

$$\theta(\xi, \eta) = \Theta_0(\eta) + \xi^{-\frac{1}{2}} \Theta_1(\eta) + \ldots$$

Similarly for the inner layer equations (21)-(23) we have

$$f(\xi,\chi)=\xi^{-1}f_0(\chi)+\xi^{-3/2}f_1(\chi)+\ldots$$

$$h(\xi,\chi)=h_0(\chi)+\xi^{-\frac{1}{2}}h_1(\chi)+\ldots \tag{26}$$

$$\theta(\xi,\chi)=\xi^{-\frac{1}{2}}\theta_0(\chi)+\xi^{-1}\theta_1(\chi)+\ldots$$

It may be easily verified that the main layer equations are given by

$$(1+\frac{\Delta}{2})F_0'''+4F_0F_0''-3(F_0')^2+\Theta_0=0 \tag{27}$$

$$(1+\frac{\Delta}{2})F_1'''+4F_0F_1''+3F_1F_0'-5F_0'F_1'+\Theta_1=0 \tag{28}$$

$$\frac{\Theta_0''}{\mathrm{Pr}}+4F_0\Theta_0'-F_0'\Theta_0=0 \tag{29}$$

$$\frac{\Theta_1''}{\mathrm{Pr}}+4F_0\Theta_1'+3F_1\Theta_0'-F_1'\Theta_1=0 \tag{30}$$

$$H_0=\frac{\Theta_0'}{4\Delta} \tag{31}$$

$$H_1=\frac{\Theta_1'}{4\Delta} \tag{32}$$

The boundary conditions are given by

$$\eta=0: \quad F_0=F_0'=0, \quad \Theta_0'=-1, \quad \Theta_1'=0$$

$$\eta\to\infty: \quad F_0'=0, \quad \Theta_0=0, \quad \Theta_1=0 \tag{33}$$

The inner layer equations are given by

$$(1+\frac{\Delta}{2})f_0'''+\Delta h_0'=0 \tag{34}$$

$$(1+\frac{\Delta}{2})f_1'''+\Delta h_1'=0 \tag{35}$$

$$(1+\Delta)h_0''-2\Delta h_0=0 \tag{36}$$

$$(1+\Delta)h_1''-2\Delta h_1=0 \tag{37}$$

$$\theta_0'' = 0 \tag{38}$$

$$\theta_1'' = 0 \tag{39}$$

The boundary conditions at $\chi = 0$ are given by:

$$\chi = 0: \quad f_0 = f_0' = f_1 = f_1' = 0, \quad h_0 = (\frac{1}{2} - n) f_0'', \quad h_1 = (\frac{1}{2} - n) f_1'', \quad \theta_0' = -1, \quad \theta_1' = 0 \tag{40}$$

The solutions are given by

$$f_0(\chi) = \frac{\chi^2}{2} F_0''(0) + \frac{2\Delta}{(2+\Delta)} \frac{c}{\lambda^2} [1 - \lambda\chi - e^{-\lambda\chi}] \tag{41}$$

Where

$$c = \frac{(1-2n)(2+\Delta)}{4(1+\Delta-n\Delta)} F_0''(0)$$

$$\lambda = \sqrt{\frac{2\Delta}{1+\Delta}} \tag{42}$$

$$h_0(\chi) = ce^{-\lambda\chi}$$

$$\theta_0(\chi) \sim -\chi \tag{43}$$

$$f_1(\chi) = \frac{\chi^2}{2} F_1''(0) + \frac{(1-2n)(2+\Delta)}{4(1+\Delta-n\Delta)} F_1''(0)(1 - \lambda\chi - e^{-\lambda\chi}) \tag{44}$$

$$h_1(\chi) = \frac{(1-2n)(2+\Delta)}{4(1+\Delta-n\Delta)} F_1''(0) e^{-\lambda\chi} \tag{45}$$

$$\theta_1(\chi) = 0 \tag{46}$$

For large values of $\xi$ and small values of $\eta$, we may write for the outer layer

$$f = \xi^{-1}[\frac{1}{2} F_0''(0)\chi^2 + F_1'(0)\chi + \ldots] + \xi^{-3/2}[\frac{1}{6} F_0''(0)\chi^3 + \frac{1}{2} F_1''(0)\chi^2 + \ldots] \tag{47}$$

For large values of $\chi$ the inner layer solution is given by

$$f = \xi^{-1}[\frac{1}{2} F_0''(0)\chi^2 - c\lambda\chi + \ldots] + \xi^{-3/2}[-\frac{\Theta_0(0)\chi^3}{3(2+\Delta)} + \frac{1}{2} F_1''(0)\chi^2 + \ldots] \tag{48}$$

From equations (47) and (48) we get

$$F_1'(0) = -c\lambda \tag{49}$$

The shear stress and heat transfer rates may be computed by the following equations:

$$\left.\frac{\partial^2 f}{\partial \eta^2}\right|_{\eta=0} = \left[\frac{\partial^2 f_0}{\partial \chi^2} + \xi^{-\frac{1}{2}} \frac{\partial^2 f_1}{\partial \chi^2} + \ldots\right]_{\chi=0} \tag{50}$$

$$\theta\,|_{\eta=0} = [\xi^{-\frac{1}{2}}\theta_0 + \xi^{-1}\theta_1]_{\chi=0} \tag{51}$$

## Discussion of results

Figures 1-3 display the distribution of velocity, angular velocity and temperature within the boundary layer. As Δ increases, we observe that the velocity maximum decreases in amplitude and the location of the maximum velocity moves farther away from the wall. The momentum and thermal

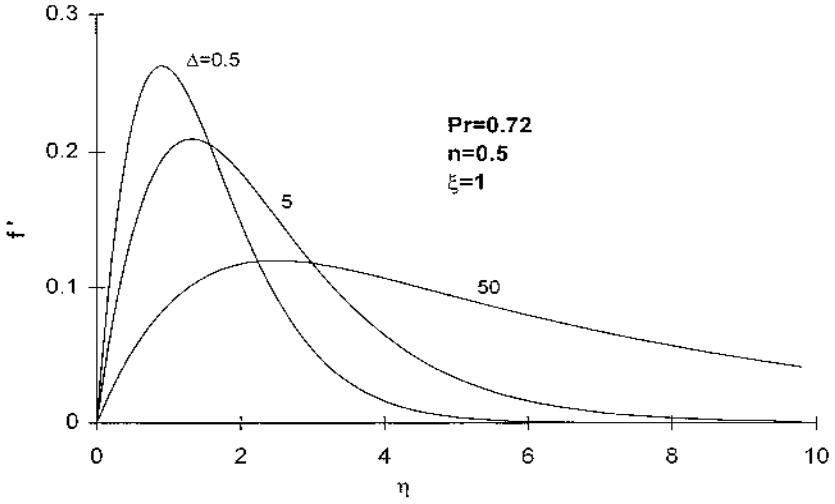


**Figure 1.**
Dimensionless streamwise velocity distribution

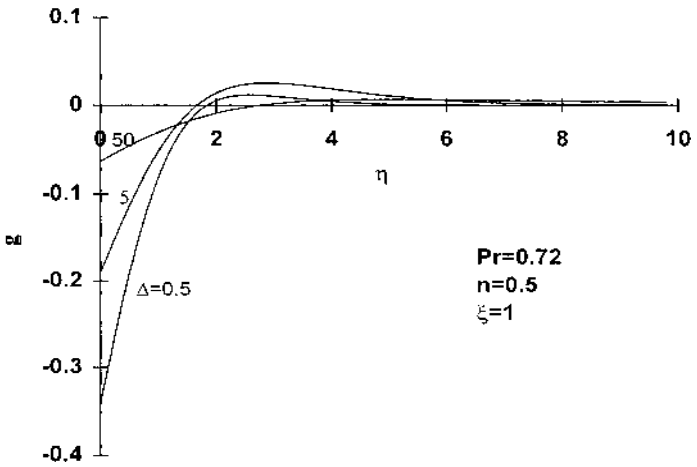


**Figure 2.**
Dimensionless microrotation distribution

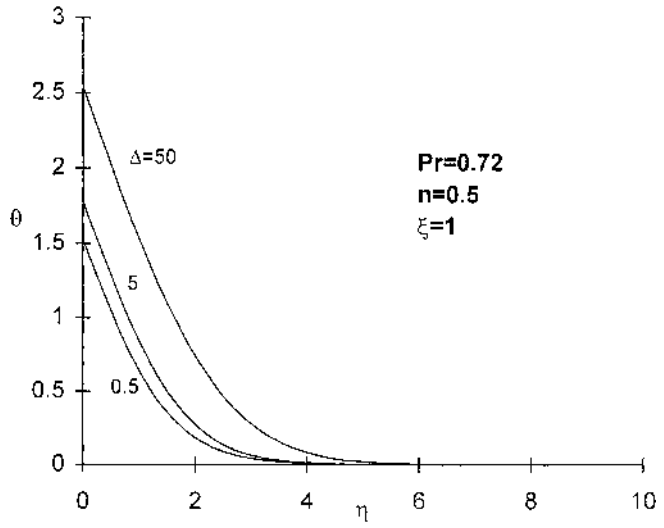


**Figure 3.** Dimensionless temperature distribution

boundary layer thicknesses increases with $\Delta$. The wall value of the microrotation component decreases monotonically to zero at the boundary layer edge. As $\Delta$ increases, we observe that the temperature within the boundary layer increases. The parameter $\Delta$ is proportional to spin gradient viscosity of the fluid microstructure. Increasing it results in flow retardation, which in turn decreases the rate of heat transfer convected away from the heated wall.

Figure 4 shows that the rates of microrotation decrease as the Prandtl number increases. The microrotation increases with $\xi$.

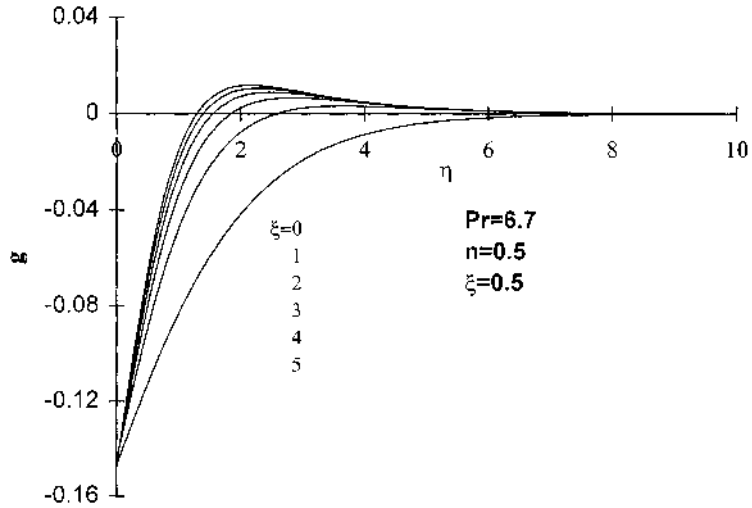


**Figure 4.** Dimensionless microrotation distribution

Figures 5 and 6 display the numerical results for the local friction factor versus $\xi$. As $n$ increases, the friction factor increases whereas as $\Delta$ increases, the friction factor tends to decrease. The friction factor decreases as the Prandtl number increases.

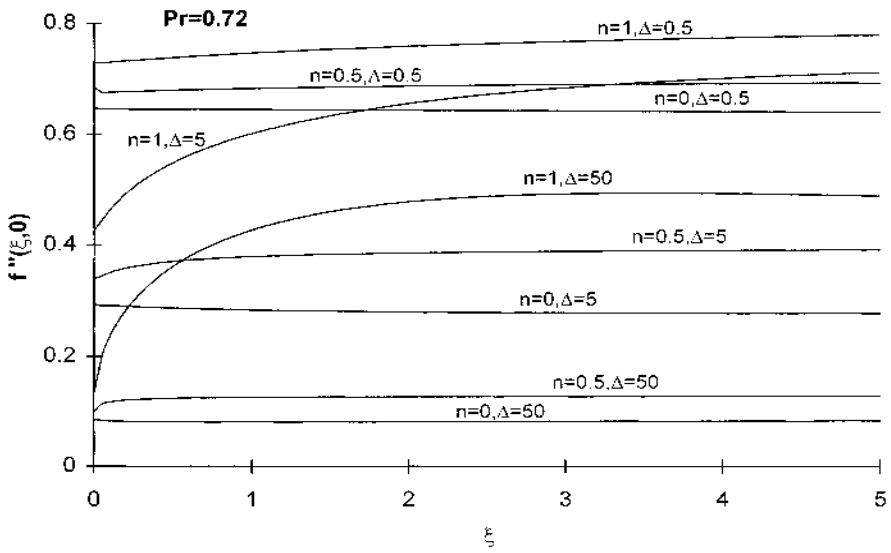


**Figure 5.**
Friction factor versus dimensionless distance $\xi$

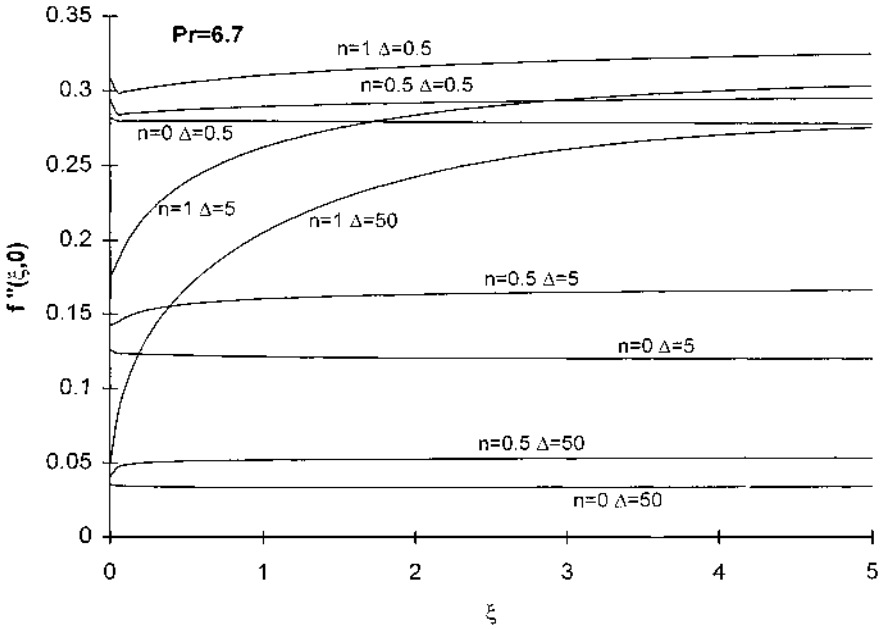


**Figure 6.**
Friction factor versus dimensionless distance $\xi$

Figures 7 and 8 show the results for the wall couple stress. As $n$ increases, the wall couple stress tends to increase whereas increasing values of $\Delta$ tend to

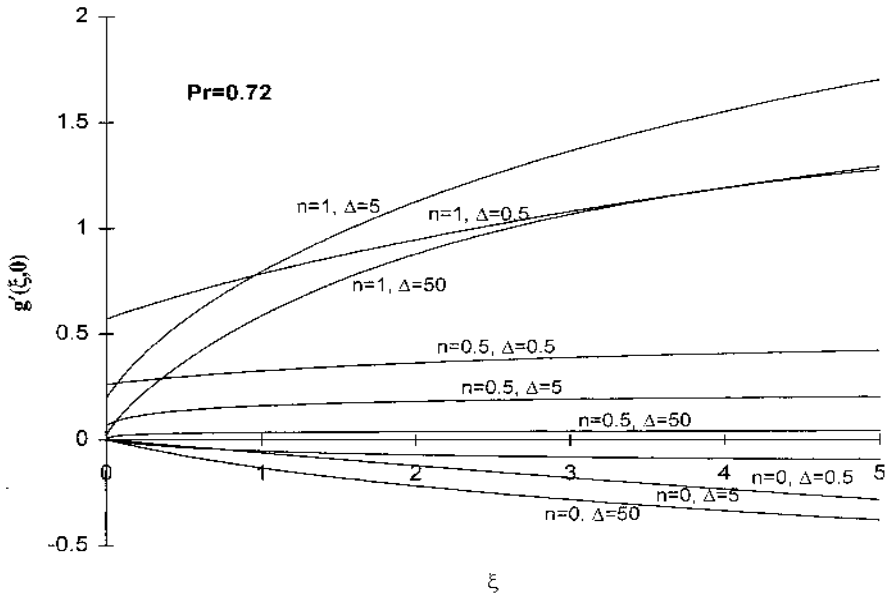


**Figure 7.**
Wall couple stress versus dimensionless distance $\xi$

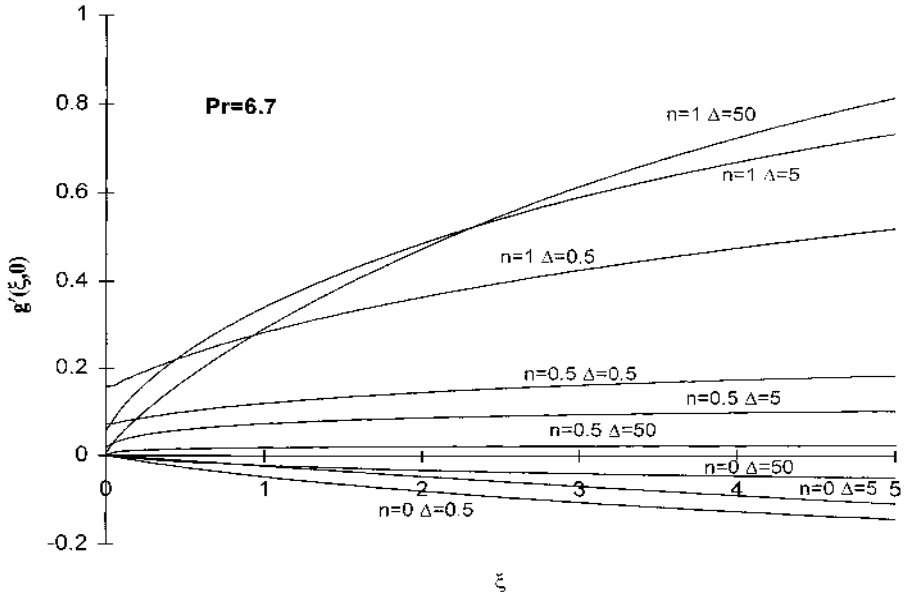


**Figure 8.**
Wall couple stress versus dimensionless distance $\xi$

decrease it. Higher values of Prandtl number result in reduced wall couple stress values.

Figures 9 and 10 show the results for the Nusselt number, we observe that Nusselt number (dimensionless wall heat transfer rate) decreases as $\Delta$

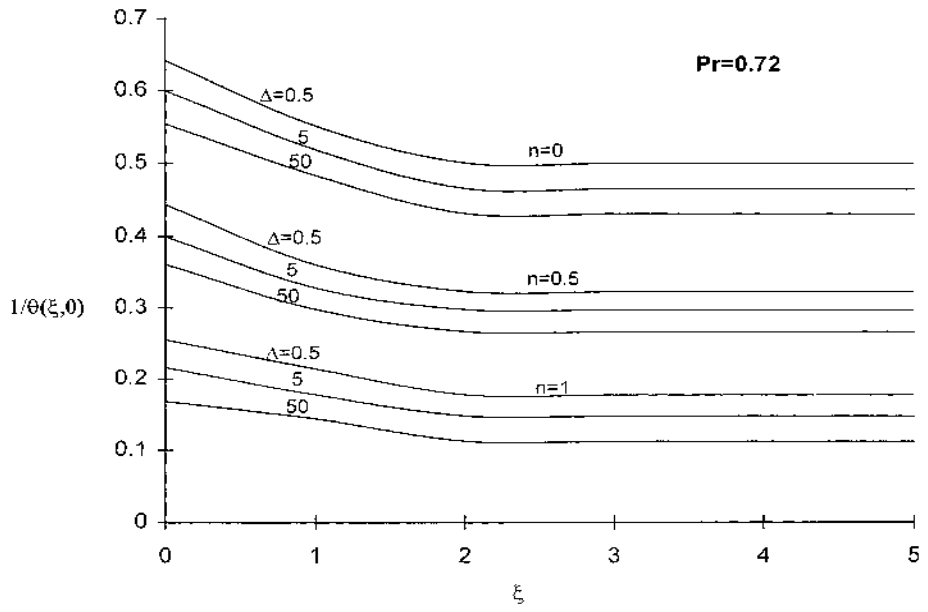


**Figure 9.**
Nusselt number versus $\xi$

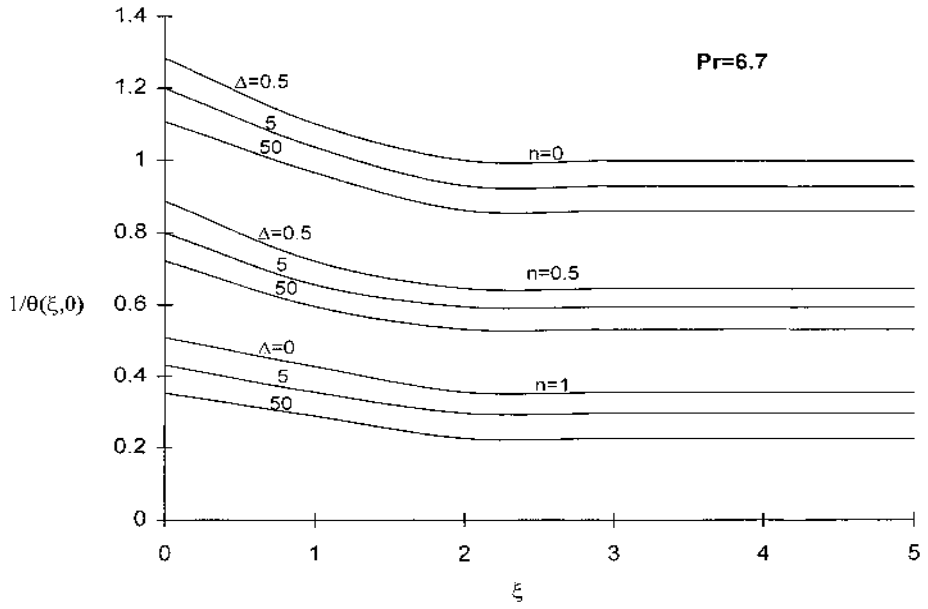


**Figure 10.**
Nusselt number versus $\xi$

increases. Similar behavior is observed as $n$ increases. The heat transfer rate increases as Prandtl number increases.

Tables I-VI display numerical results for the asymptotic solution for large distances away from the leading edge. These results are plotted together with

| $\Delta$ | $F_0''(0)$ | $F_1''(0)$ | $\theta(0)$ | $\theta_1(0)$ |
|---|---|---|---|---|
| 0.5 | 0.7177 | 0.4158 | 1.5278 | 0.3402 |
| 5 | 0.3996 | 0.1892 | 1.7591 | 0.3765 |
| 50 | 0.1257 | 0.0337 | 2.4578 | 0.3572 |

**Table I.** Pr = 0.72 $n$ = 0

| $\Delta$ | $F_0''(0)$ | $F_1''(0)$ | $\theta(0)$ | $\theta_1(0)$ |
|---|---|---|---|---|
| 0.5 | 0.7177 | 0 | 1.5278 | 0 |
| 5 | 0.3996 | 0 | 1.7591 | 0 |
| 50 | 0.1257 | 0 | 2.4578 | 0 |

**Table II.** Pr = 0.72 $n$ = 0.5

| $\Delta$ | $F_0''(0)$ | $F_1''(0)$ | $\theta(0)$ | $\theta_1(0)$ |
|---|---|---|---|---|
| 0.5 | 0.7177 | –0.6237 | 1.5278 | –0.5103 |
| 5 | 0.3996 | –1.1355 | –2.2592 | –2.2592 |
| 50 | 0.1257 | –1.7204 | 2.4578 | –18.215 |

**Table III.** Pr = 0.72 $n$ = 1

| $\Delta$ | $F_0''(0)$ | $F_1''(0)$ | $\theta(0)$ | $\theta_1(0)$ |
|---|---|---|---|---|
| 0.5 | 0.3133 | 0.2379 | 0.8740 | 0.3402 |
| 5 | 0.1723 | 0.1127 | 1.0477 | 0.3765 |
| 50 | 0.0528 | 0.0210 | 1.5310 | 0.3571 |

**Table IV.** Pr = 6.7 $n$ = 0

| $\Delta$ | $F_0''(0)$ | $F_1''(0)$ | $\theta(0)$ | $\theta_1(0)$ |
|---|---|---|---|---|
| 0.5 | 0.3133 | 0 | 0.8740 | 0 |
| 5 | 0.1723 | 0 | 1.0477 | 0 |
| 50 | 0.0528 | 0 | 1.5310 | 0 |

**Table V.** Pr = 6.7 $n$ = 0.5

| $\Delta$ | $F_0''(0)$ | $F_1''(0)$ | $\theta(0)$ | $\theta_1(0)$ |
|---|---|---|---|---|
| 0.5 | 0.3133 | –0.3568 | 0.8740 | –0.5103 |
| 5 | 0.1723 | –0.6763 | 1.0477 | –2.2593 |
| 50 | 0.0528 | –1.0716 | 1.5310 | –18.214 |

**Table VI.** Pr = 6.7 $n$ = 1

numerical results of the nonsimilar problem presented in Figures 5-10. In all cases, the agreement between the numerical and asymptotic solution is very good.

## Concluding remarks

In this paper, we have presented a boundary layer analysis for the flow of a micropolar fluid over a vertical plate with uniform surface heat flux conditions. The governing equations are transformed into a set of nonsimilar parabolic equations where numerical solution has been presented for a wide range of parameters. An asymptotic solution is presented for large distances from the leading edge of the plate. The numerical results indicated that the micropolar fluids reduce drag and surface heat transfer rate.

### References

Eringen, A.C. (1966), "Theory of micropolar fluids", *Journal of Math. Mech.* Vol. 6, pp. 1-18.

Eringen, A.C. (1972), "Theory of thermomicrofluids", *Math. Anal. Appl. Journal,* Vol. 38, pp. 480-96

Gorla, R.S.R. (1983), "Heat transfer in micropolar boundary layer flow over a flat plate", *International Journal of Engineering Science,* Vol. 21, pp. 791-6.

Gorla, R.S.R., Lee, J.K., Nakamura, S. and Pop, I. (1993), "Effect of transverse magnetic field on mixed convection in a wall plume of power law fluids", *International Journal of Engineering Science,* Vol. 31, pp. 1035-45.

Jena, S.K. and Mathur, M.M. (1981), "Similarity solutions for laminar free convective flow of a thermomicropolar fluid past a nonisothermal vertical plate", *International Journal of Engineering Science,* Vol. 19, pp. 1431-9.

Rees, D.A.S. and Bassom, A.P. (1996), "The Blasius boundary-layer flow of a micropolar fluid", *International Journal of Engineering Science,* Vol. 34, pp. 113-24.